Materials Transactions, Vol. 55, No. 2 (2014) pp. 275 to 284

Prediction of the Constitutive Equation for Uniaxial Creep of a Power-Law Material through Instrumented Microindentation Testing and Modeling*1

Hidenari Takagi[1], Ming Dao[2] and Masami Fujiwara[1,*2]

[1]*Division of Applied Physics, Department of General Education, College of Engineering, Nihon University, Koriyama 963-8642, Japan*
[2]*Department of Materials Science and Engineering, School of Engineering, Massachusetts Institute of Technology, Massachusetts 02139, USA*

Indentation creep tests and finite element simulations were performed on a model material to show that the constitutive equation for conventional uniaxial creep can be derived using the instrumented indentation testing technique. When the indentation pressure and the indentation creep rate are maintained at constant values of p_s and $\dot{\varepsilon}_{in(s)}$, respectively, the contours of the equivalent stress and the equivalent plastic strain rate in the region beneath the conical indenter expand according to the increase in the displacement of the indenter while maintaining geometrical self-similarity. These findings indicate that a pseudo-steady deformation state takes place around the indenter tip. The representative point exhibiting the creep behavior within the limited region, which actually determines the indenter velocity, is defined as the location where the equivalent stress $\bar{\sigma}_r$ equals $p_s/3$. The equivalent plastic strain rate $\dot{\bar{\varepsilon}}_r$ at this point is found to be $\dot{\varepsilon}_{in(s)}/3.6$ in the case when the stress exponent for creep is 3. The stress exponent and the activation energy for creep extracted from the results of Al–5.3 mol%Mg solid-solution alloy indentation tests are in close agreement with those of tensile creep tests reported in the literature. In addition, the values for $\bar{\sigma}_r$ and $\dot{\bar{\varepsilon}}_r$ agree well with the values for the applied stress and the corresponding creep rate in tensile creep tests at the same temperature. The above results show that the creep characteristics of advanced materials, which are often available in minute quantities or as small-volume specimens, can be obtained from carefully designed indentation creep tests, and furthermore the constitutive equation for tensile creep can be predicted with sufficient accuracy through indentation creep test results. [doi:10.2320/matertrans.M2013370]

(Received September 27, 2013; Accepted November 8, 2013; Published December 20, 2013)

Keywords: *indentation, conical indenter, finite element method, creep, pseudo-steady-state, control volume, representative point, stress exponent, activation energy, creep-rate controlling mechanism*

1. Introduction

The indentation hardness test is a mechanical testing method that has been used for more than a hundred years to evaluate material strength by the size of an impression formed when a rigid indenter is pressed at a constant load into a sample surface.[1,2] Following recent progress in nano- and micro-scale mechanical properties research and associated technologies, there is interest in the instrumented indentation testing technique, which was developed from conventional hardness testing methods.[3–5] In this testing technique, changes in load and indenter displacement over time are measured when an indenter tip is pressed into a sample in various loading modes, and elastic characteristics such as Young's modulus and creep characteristics such as the stress exponent are evaluated. This method is classified as either nanoindentation (NanoIn) testing[4] or microindentation (MicroIn) testing[5] depending on the degree of indentation depth. The former is usually used to examine room-temperature mechanical characteristics of thin film materials, nanostructures, and so forth, while the latter is often used for studying high-temperature mechanical characteristics of small-volume specimens and functionally graded materials.

For high-temperature structural materials, it is important to determine the constitutive equation for creep with regard to creep rate, stress, temperature, and material structure. A certain sample size is required to obtain this equation because tensile creep tests must be performed under a minimum of three stress conditions per temperature. However, for structural members that are in use or heat-resistant materials under development, oftentimes only a tiny sample can be obtained for testing and ordinary tensile creep tests cannot be conducted enough times if not impossible. Thus, it is extremely advantageous if the constitutive equation for creep can be obtained by MicroIn testing under these circumstances.

We will first look at trends in research on MicroIn creep testing and assess the relationship between the present work and the existing literatures in the followings.

1.1 Extraction of creep characteristics

Mulhearn and Tabor[6] determined indentation creep rate from the change in impression size with respect to loading time ($\equiv \dot{d}/d$, where d is the impression diameter of the spherical indenter, and $\dot{d}$ is the time rate of change of the impression diameter). They determined the creep characteristic values of low-melting-point metals under the assumption that a power law relation holds true between indentation creep rate and hardness. Chu and Li[7] used an indentation tester that could continuously measure indentation depth of a cylindrical indenter under constant load to determine the creep characteristic values of β-tin single crystals under the assumption that a power law relation holds true between the indenter velocity and the indentation pressure. In these papers, a power law relation for tensile creep, known to hold true under steady-state deformation, was taken as a presumed condition for creep analysis without taking into consideration the strain gradient under the indenter. To resolve this issue, Sargent and Ashby[8] studied the case in which the strain contour line pattern under the indenter maintains geometrical self-similarity. They derived a constitutive equation for

*1This Paper was Originally Published in Japanese in J. Japan Inst. Metals **76** (2012) 597–606.
*2Corresponding author, E-mail: fujiwara@ge.ce.nihon-u.ac.jp

indentation creep under the assumption that the indentation creep rate ($\equiv \dot{u}/\sqrt{A}$, where $\dot{u}$ is the indenter velocity, and A is the horizontal projected area of Vickers impression) is proportional to the equivalent plastic strain rate $\dot{\bar{\varepsilon}}$ under the indenter, and the hardness value is proportional to the equivalent stress $\bar{\sigma}$ under the indenter. However, it was ambiguous what values under the indenter are indicated by $\dot{\bar{\varepsilon}}$ and $\bar{\sigma}$. An indentation creep tester that can be used at up to about 1000 K was developed at the authors' laboratory,[9] and constant-load indentation tests and load-jump tests were conducted using a conical indenter on pure metals, eutectic alloys, solid-solution alloys, and precipitation-strengthened alloys.[10–13] In addition, they simulated the process of pressing a conical indenter into a power-law material using the finite element (FE) method, and confirmed that when the indentation pressure p and indentation creep rate $\dot{\varepsilon}_{\mathrm{in}}$ became constant, the contour line pattern of $\dot{\bar{\varepsilon}}$ under the indenter expanded while maintaining self-similarity.[14]

1.2 Indentation loading method

Lucas and Oliver[15] demonstrated that when the load is increased exponentially, indentation pressure asymptotically approaches a constant value as time elapses. Further, Cheng and Cheng[16] carried out a dimensional analysis in which a sharp indenter was pressed into a power-law material and obtained results similar to those of Lucas *et al.*

1.3 Methods of predicting the constitutive equation for tensile creep from MicroIn tests

Hyde *et al.*[17] performed FE simulation of pressing a cylindrical indenter under constant load into a power-law material and numerically evaluated the proportionality constants, C_1 and C_2, in $\bar{\sigma} = C_1 p$ and $\dot{\bar{\varepsilon}} = C_2 \dot{\varepsilon}_{\mathrm{in}}$ (where C_1 and C_2 conform to the symbolic convention of the present paper) under the hypothesis that they are not dependent on the stress exponent for creep. Bower *et al.*[18] performed theoretical analysis and FE simulations of the same problem and determined the values of C_1 and C_2 under the hypothesis that the equivalent plastic strain rate is expressed by $\dot{\bar{\varepsilon}} = \dot{u}/a$ (where a is the true contact radius of the indenter). They showed that the obtained values were all dependent on the stress exponent. Thus, the results of the two research groups were distinctively different, and a method for deriving these proportionality constants has not yet been established. We have not yet reached the point where the constitutive equation for tensile creep (including all the creep parameter) can be accurately predicted by an indentation creep test.

The objective of this study is to demonstrate that the constitutive equation for conventional tensile creep or uniaxial creep can be predicted with sufficient accuracy from constant-pressure indentation creep test results. To achieve this objective, we theoretically derived the constitutive equation of indentation creep for the pseudo-steady deformation state and performed MicroIn testing and FE simulation. We then performed the following six research tasks.

(1) Using FE simulation, we clarified that a pseudo-steady deformation state occurs exactly under the indenter when a conical indenter is pressed at a constant pressure.
(2) We estimated a region in which the indenter velocity had been substantially determined (control volume, CV), and studied the factors that influenced the magnitude thereof.
(3) We defined a point within the CV that represented deformation behavior, determined the equivalent stress and equivalent plastic strain rate at this CV representative point, and examined the relationship between indentation pressure and indentation creep rate.
(4) We derived the constitutive equation for the indentation creep of a power-law material and examined methods for extracting creep characteristics for a region of material near the CV representative point through MicroIn testing.
(5) We selected an Al–Mg solid-solution alloy as a model material, and performed MicroIn testing on it. We compared the obtained creep characteristic values with the tensile creep test results reported by other researchers.
(6) From the results of MicroIn testing and FE simulation, we derived the constitutive equation for conventional tensile creep or uniaxial creep. We compared this constitutive equation with those for tensile creep derived by other researchers.

2. Computational and Experimental Methods

2.1 Elasto-plastic finite element simulation

FE simulations of indentation creep were performed using the general-purpose non-linear FE program ABAQUS Standard (SIMULIA) into which our own subroutines were incorporated. A cylindrical model of a perfectly elastic plastic body was created using four-noded bilinear axisymmetric quadrilateral elements, and a rigid indenter (apex angle: 136°) was vertically pressed into the center of the top surface thereof. The cylindrical model was 3 mm in diameter and 3 mm high, and the maximum indenter displacement was 0.15 mm. We assumed no friction between the indenter and the sample surface and that elastic deformation and power-law creep ($\dot{\bar{\varepsilon}} = B\bar{\sigma}^n$, where $\dot{\bar{\varepsilon}}$ is the equivalent plastic strain rate, B is the creep constant, $\bar{\sigma}$ is the equivalent stress, and n is the stress exponent for creep) occurring in the finite elements. The elastic characteristics used were Young's modulus $E = 37.8\,\mathrm{GPa}$[19] and Poisson's ratio $\nu = 0.345$,[20] and the creep characteristic values $B = 1.0 \times 10^{-6}$ $\mathrm{MPa^{-3}\,s^{-1}}$, and $n = 3.0$[12] were used. The details of the FE model have been reported elsewhere.[12]

2.2 Indentation creep test

An ingot of Al–5.3 mol% Mg alloy was homogenized in an argon atmosphere for 86.4 ks at 773 K (0.85 T_{m}, where T_{m} is the absolute melting point). The ingot was then cut into 5 mm × 10 mm × 5 mm cuboids, which were adjusted by emery polishing to ensure that the 5 mm × 10 mm test surface and the bottom surface were parallel. Then, they were annealed for 3.6 ks at 773 K. Immediately before indentation creep test, approximately 40 μm of the sample surface layer was removed by electropolishing. Details of sample preparation have been reported elsewhere.[13]

Indentation creep tests were performed in an argon atmosphere using a microindenter (ULVAC-RIKO, Inc.,

Japan). The apex angle of the diamond conical indenter used was 136°. The test temperature was 636–773 K (0.70–0.85 T_m), and the temperature fluctuation during the indentation creep tests was ±1 K or less. The indentation load was applied by an electromagnetic force, and indenter displacement was measured by a linear variable-differential transformer. Here, the measurement precision of load and displacement were 10^{-2} N and 10^{-7} m, respectively. The measurement data were recorded by a personal computer at a sampling rate of $10\,s^{-1}$.

3. Constitutive Equation for Indentation Creep

3.1 Constraint factor

When a conical indenter is pressed vertically into a sample surface with load F, if piling-up and sinking-in of the surface and the effect of friction are ignored, the indentation pressure p can be expressed as:

$$p = \frac{F}{\pi u^2 \tan^2\theta}. \tag{1}$$

Here, u is indenter displacement, which expresses the indentation depth from the original surface, and θ is the half-apex angle. When F is kept constant under static or quasi-static conditions, the indenter is at the location where the indentation load and deformation resistance force are in equilibrium.

Hill *et al.*[21] analyzed using the slip-line field method the case in which a triangular indenter was pressed into a two-dimensional semi-infinite block of a perfectly rigid plastic body. They demonstrated that the yield stress Y is proportional to p, and when $\theta = 68°$, $C_1 = 1/2.4$. Cheng and Cheng[22] performed dimensional analysis assuming that C_1 is dependent on Young's modulus, yield stress, and work-hardening rate, and they demonstrated that in a perfectly rigid plastic body, $C_1 \cong 1/2.8$. Kudo[23] showed that when the static friction coefficient between the indenter and sample is 0.1 to 0.2, $C_1 \cong 1/2.9$ to $1/2.8$. Tabor *et al.*[2] discovered that the relationship $Y \cong H/3$ holds true between Vickers hardness H and flow stress Y corresponding to tensile strain $\varepsilon = \varepsilon_0 + 0.08$ (where ε_0 is the initial strain). Nakamura *et al.*[24] demonstrated that the relationship $Y \cong H/2.8$ holds true for flow stress corresponding to compression strain $\varepsilon = 0.08$, and asserted that this Y value corresponds to the average combined stress that occurs under the indenter. As described above, the theoretical and experimental results for indentation deformation show that the hardness value (indentation pressure) is proportional to the flow stress. In the present paper as well, the relationship $\bar{\sigma}_r = C_1 p$ holds true between the indentation pressure p and the representative equivalent stress $\bar{\sigma}_r$ under the indenter. Hereinafter, we shall refer to C_1 as the constraint factor, which will be assumed to be $1/3$.

3.2 Control volume

The control volume (CV) means the region in which the indenter velocity has been substantially determined. Here, the location that represents the creep behavior of that region will be called the CV representative point, at which the equivalent stress is equal to $p/3$, and this stress value shall be referred to as the representative stress, $\bar{\sigma}_r$:

$$\bar{\sigma}_r = p/3. \tag{2}$$

The equivalent plastic strain rate at this point shall be referred to as the representative strain rate $\dot{\bar{\varepsilon}}_r$.

Let us consider the case in which the contour lines of the equivalent plastic strain rate expand exactly under the indenter while maintaining self-similarity. This means that when indenter displacement is doubled, the magnitude of the expansion of these contour lines doubles as well, while contour line shapes remain unchanged. According to this scaling rule, the indentation creep rate that provides a measure of the rate of CV expansion is defined as:[22,25]

$$\dot{\varepsilon}_{in} = \dot{u}/u. \tag{3}$$

Here, u is the indenter displacement, and $\dot{u}$ is the indenter velocity. For compatibility, the following relationship should hold true between $\dot{\varepsilon}_{in}$ and the representative strain rate $\dot{\bar{\varepsilon}}_r$:

$$\dot{\bar{\varepsilon}}_r = C_2 \dot{\varepsilon}_{in}, \tag{4}$$

where C_2 is the conversion coefficient for determining $\dot{\bar{\varepsilon}}_r$.

3.3 Pseudo-steady deformation state and creep characteristic values

In steady-state deformation of crystalline materials, it is known that the following power law (Norton's law) holds true between the equivalent stress $\bar{\sigma}$ and the equivalent plastic strain rate (creep rate) $\dot{\bar{\varepsilon}}$:

$$\dot{\bar{\varepsilon}} = A_1 \left(\frac{\bar{\sigma}}{E}\right)^n. \tag{5}$$

Here, $A_1 = A_0 \exp(-Q/RT)$, A_0 is the creep constant, Q is the activation energy for creep, R is the gas constant, T is the test temperature, E is Young's modulus at each temperature, and n is the stress exponent for creep. Therefore, the constitutive equation for indentation creep is written as:

$$\dot{\varepsilon}_{in} = A_2 \left(\frac{p}{E}\right)^n = A_3 \left(\frac{F}{Eu^2}\right)^n. \tag{6}$$

Here, $A_2 = A_1 C_1^n / C_2$, and $A_3 = A_2/(\pi \tan^2\theta)^n$.

When the strain hardening rate and recovery rate are in equilibrium in the CV during indentation creep, deformation proceeds under the conditions where p and $\dot{\varepsilon}_{in}$ are constant. In this case, $F \propto u^2$, and $\dot{\varepsilon}_{in} = d \ln u/dt = \alpha$ (constant). In order for both to hold true, the indentation load F must be given by:

$$F = F_0 \exp(2\alpha t). \tag{7}$$

Here, F_0 is the initial load, α is the load increment parameter, and t is the loading time. From eqs. (6) and (7), the change over time of the indenter displacement u—that is, the indentation creep curve—is expressed by the following:

$$u = \sqrt{\frac{F_0}{E}\left[\frac{A_3}{\alpha}\{\exp(2\alpha n t) - 1\}\right]^{1/n}}. \tag{8}$$

The above equation shows that indenter displacement increases as temperature increases via A_3. The indentation creep rate $\dot{\varepsilon}_{in}$ is expressed by:

$$\dot{\varepsilon}_{in} = \frac{\alpha}{1 - \exp(-2\alpha n t)}. \tag{9}$$

The above equation shows that indentation creep rate is not temperature-dependent. Furthermore, the indentation pressure p is expressed by the following:

$$p = E\left[\frac{\alpha}{A_2\{1-\exp(-2\alpha n t)\}}\right]^{1/n}. \tag{10}$$

The above equation shows that indentation pressure decreases as temperature increases via A_2. From eqs. (9) and (10), it is seen that $\dot{\varepsilon}_{\mathrm{in}}$ and p asymptotically approach constant values as time elapses, and the larger the value of n, the shorter the time to reach a constant value. When the individual constants are expressed as $\dot{\varepsilon}_{\mathrm{in(s)}}$ and p_{s}, they may be written as:

$$\dot{\varepsilon}_{\mathrm{in(s)}} \cong \alpha, \tag{11}$$

$$p_{\mathrm{s}}/E \cong (\alpha/A_2)^{1/n}. \tag{12}$$

$\dot{\varepsilon}_{\mathrm{in(s)}}$ is not temperature-dependent; however, p_{s}/E decreases as temperature increases.

When the indenter is pressed with an indentation pressure of p_{s} and indentation creep rate of $\dot{\varepsilon}_{\mathrm{in(s)}}$, the pseudo-steady deformation state is realized, as will be described later. From eqs. (2) and (4), the representative stress $\bar{\sigma}_{\mathrm{r}}$ and representative strain rate $\dot{\bar{\varepsilon}}_{\mathrm{r}}$ at this time are given by $\bar{\sigma}_{\mathrm{r}} = C_1 p_{\mathrm{s}}$ and $\dot{\bar{\varepsilon}}_{\mathrm{r}} = C_2 \dot{\varepsilon}_{\mathrm{in(s)}}$. From eq. (5), the stress exponent for creep, n, of a material small block near the CV representative point is:

$$n = \left.\frac{\partial \ln \dot{\varepsilon}_{\mathrm{in(s)}}}{\partial \ln(p_{\mathrm{s}}/E)}\right|_T. \tag{13}$$

The activation energy for creep Q is given by:

$$Q = -R\,\frac{\partial \ln \dot{\varepsilon}_{\mathrm{in(s)}}(E/p_{\mathrm{s}})^n}{\partial(1/T)}. \tag{14}$$

4. Results and Discussion

4.1 FE Simulation of indentation creep

By FE simulation, we examined the state of deformation when a conical indenter is pressed into a power-law creep material. The indentation load is given by $F = F_0 \exp(2\alpha t)$, where $F_0 = 0.29\,\mathrm{N}$ and $\alpha = 2.5 \times 10^{-4} - 4.0 \times 10^{-3}\,\mathrm{s}^{-1}$. Figure 1 shows the change in indenter displacement over time (open circles) at $\alpha = 5.0 \times 10^{-4}\,\mathrm{s}^{-1}$. For convenience, only data measured every 100 s is plotted. Immediately after loading, an instantaneous indenter displacement u_0 occurred due to elasto-plastic deformation in the region exactly under the indenter. Subsequently, indenter displacement increased in a sigmoidal shape as loading time elapsed. In the figure, the indentation creep curve for a perfectly rigid plastic body obtained from eq. (8) is shown as a thick line. The values $A_1 = 5.40 \times 10^7\,\mathrm{s}^{-1}$, $C_1 = 1/3$, and $C_2 = 1/3.6$ (to be described later) were used in the calculation. This curve agrees well with the FE simulation results for a perfectly elasto-plastic body (open circles). This finding demonstrates that the influence of elastic deformation on the indentation creep curve is negligibly small.

Figure 2 shows as open circles the changes over time in the indentation creep rate and indentation pressure obtained from the indentation creep curve (Fig. 1). Both decreased rapidly for the first 500 s, but they asymptotically approached the respective constant values $\dot{\varepsilon}_{\mathrm{in(s)}}$ and p_{s} at approximately

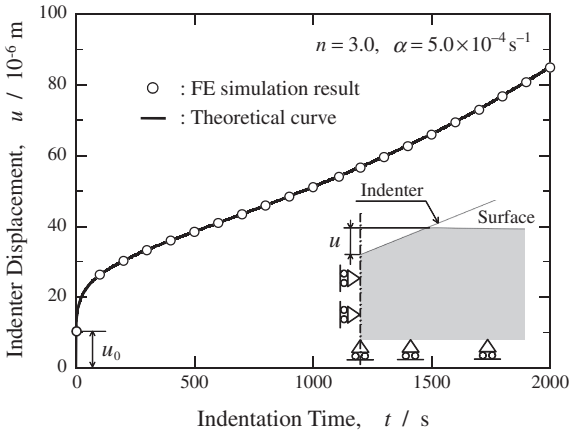

Fig. 1 Time dependence of indenter displacement obtained from FE simulations (open circles) and the indentation creep curve (solid line) derived from pseudo-steady-state indentation theory. The FE model is shown schematically at the lower right.

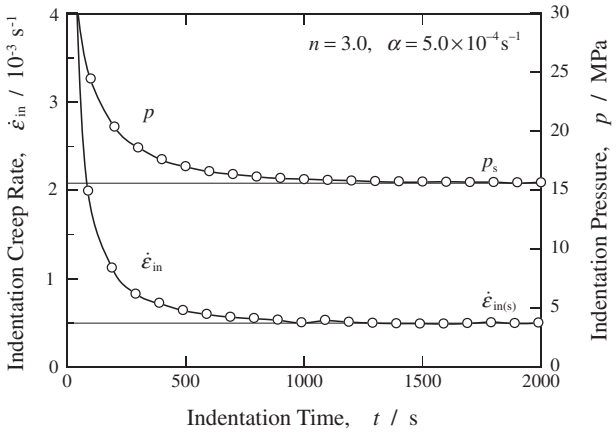

Fig. 2 Time dependence of indentation pressure and indentation creep rate. Both asymptotically approach constant values of p_{s} and $\dot{\varepsilon}_{\mathrm{in(s)}}$, respectively, after a certain loading duration.

1000 s. In this case, $\dot{\varepsilon}_{\mathrm{in(s)}} \cong 5.0 \times 10^{-4}\,\mathrm{s}^{-1}$, and $\dot{\varepsilon}_{\mathrm{in(s)}} \cong \alpha$ of eq. (11) holds true. Furthermore, $p_{\mathrm{s}} \cong 15.6\,\mathrm{MPa}$, which agrees well with $p_{\mathrm{s}} \cong E(\alpha/A_2)^{1/n} = 15.5\,\mathrm{MPa}$ of eq. (12). These results demonstrate that eqs. (11) and (12) are valid. This suggests that by knowing the relationship between $\dot{\varepsilon}_{\mathrm{in(s)}}$ and p_{s}, the stress exponent set in the FE model can be accurately extracted from eq. (13). Actually, it has been confirmed that the same value as the stress exponent ($n = 3.0$) set in the FE model is evaluated from the slope of the straight line obtained by double-logarithmically plotting $\dot{\varepsilon}_{\mathrm{in(s)}}$ and p_{s}/E.[14] The above finding demonstrates that the creep characteristic values of a material small block at the CV representative point can be accurately extracted using eqs. (13) and (14) from the experimental results of constant-pressure indentation creep test.

4.2 Self-similarity of contour line pattern of equivalent plastic strain

Figure 3(a) shows the contour line pattern (right) of equivalent plastic strain $\bar{\varepsilon}$ occurring beneath the indenter at 1600 s in Fig. 1. The dash-dot line represents the center line passing through the tip of the conical indenter, and the diagonal lines represent the exterior shape of the conical

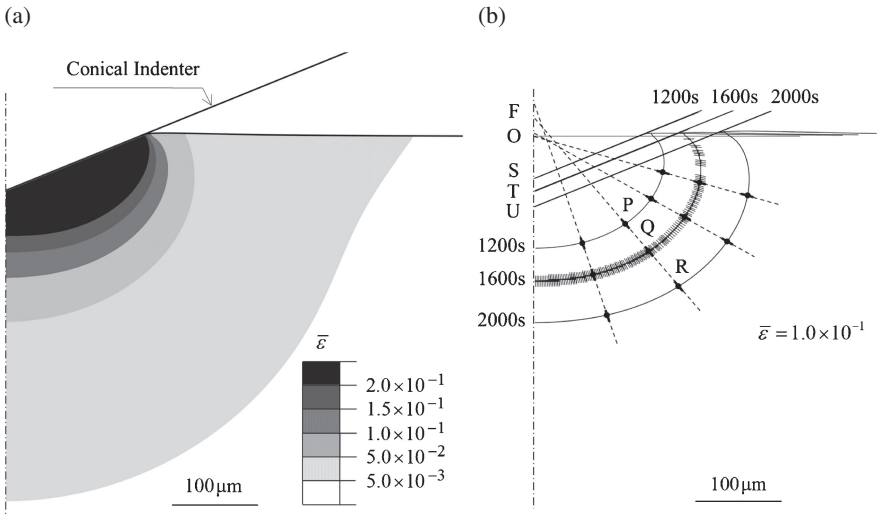

Fig. 3 (a) Contours of equivalent plastic strain $\bar{\varepsilon}$. Loading time is 1600 s. (b) Tracing of a contour line for $\bar{\varepsilon} = 1.0 \times 10^{-1}$. The short straight lines on the contour line for 1600 s indicate the direction of maximum compressive stress at the corresponding points.

indenter. A large strain of $\bar{\varepsilon} \geq 2.0 \times 10^{-1}$ occurs exactly under the indenter during indentation creep, but at a distance 3 times the radius of the impression from its center, the strain is $\bar{\varepsilon} \leq 5.0 \times 10^{-3}$. This shows that deformation due to indentation is concentrated in a very limited region beneath the indenter.

Figure 3(b) shows a tracing of the movement of the contour line of $\bar{\varepsilon} = 1.0 \times 10^{-1}$ in Fig. 3(a). As the loading time elapses from $t = 1200$ to 2000 s, the contour lines expand toward the interior of the sample like ripples on the surface of water. On the contour line at 1600 s, the principal direction of each point is represented by a short straight line toward the direction where maximum compressive strain occurs. Line RQPF is drawn by connecting point Q on this contour line with point P at 1200 s and point R at 2000 s, which have the same principal direction as point Q. In the figure, the 4 lines obtained in this manner are shown as dashed lines. The more gradual the slope of these lines, the closer to the origin O they intersect with the center line. In the pseudo-steady deformation state, there is regularity in the expansion direction of the $\bar{\varepsilon}$ contour lines because the intersection points of F and so forth are immobilized. Now, let us examine the relationship between the expansion direction and indenter displacement. The position of the indenter tip is marked as S at 1200 s, T at 1600 s, and U at 2000 s. When the ratio $\beta = \overline{SU}/\overline{ST}$ is determined, it is $\beta = 2.33$. The ratio of movement distances of the corresponding contour lines $\gamma = \overline{PR}/\overline{PQ}$ is determined. The average value of γ of the 4 lines is $\gamma = 2.33 \pm 0.05$. This result indicates that the relationship $\beta = \gamma$ holds true within the range of error. This shows that during the pseudo-steady deformation state, the $\bar{\varepsilon}$ contour line pattern expands while maintaining geometrical self-similarity as the indenter displacement increases. This result also supports the fact that the indentation creep rate can be expressed by eq. (3).

4.3 Pseudo-steady deformation state

In Fig. 4, the top level (a) illustrates the contour line pattern of equivalent stress at 1200, 1600 and 2000 s of Fig. 1, and the bottom level (b) illustrates the contour line pattern of equivalent plastic strain rate at the same points in time. If we examine the relationship between the indenter displacement and the expansion direction of each contour line pattern, the ratio κ of the indenter displacement at each point in time with respect to $t = 1600$ s is $\kappa = 0.82$ at 1200 s, and $\kappa = 1.2$ at 2000 s. Next, if we shrink or enlarge the contour line pattern at 1600 s by κ and overlay it on that contour line pattern, we ascertain that they are in complete agreement. When this scaling rule holds true, if we take the indenter tip as the origin and normalize the coordinates with respect to the indenter displacement, $\bar{\sigma}$ and $\dot{\bar{\varepsilon}}$ maintain the same values at each coordinate during indentation creep test. That is to say, in indentation creep testing, the pseudo-steady deformation state is realized around the conical indenter when the indentation pressure and indentation creep rate are constant.

4.4 Control volume and representative points

Figure 5(a) shows only the contour lines for $\bar{\sigma} = 5.0$ to 5.4 MPa among the equivalent stresses at 1600 s of Fig. 1. From Fig. 2, the indentation pressure at this time is $p_s = 15.6$ MPa. From eq. (2), the representative stress of the CV is $\bar{\sigma}_r = 5.2$ MPa. In the figure, the places where a $\bar{\sigma}_r$ value occurs, namely the CV representative points, are indicated by a thick continuous line. In three-dimensional space, a shallow-bowl-shaped CV representative surface exists in the region beneath the indenter. Figure 5(b) shows only the contour lines of $\dot{\bar{\varepsilon}} = 1.2 \times 10^{-4}$ to $1.6 \times 10^{-4}\,s^{-1}$ among the equivalent plastic strain rates of the same region as Fig. 5(a). As illustrated in the figure, the equivalent plastic strain rate at the CV representative points—that is, the representative strain rate—is $\dot{\bar{\varepsilon}}_r = 1.4 \times 10^{-4}\,s^{-1}$. Since the indentation creep rate is $\dot{\varepsilon}_{in(s)} \cong 5.0 \times 10^{-4}\,s^{-1}$, conversion coefficient C_2 of eq. (4) is as follows:

$$C_2 = 1/3.6 \text{ (when the stress exponent for creep } n = 3.0). \tag{15}$$

Here, C_2 depends on stress exponent for creep but does not depend on test conditions such as temperature. Details will be described elsewhere.

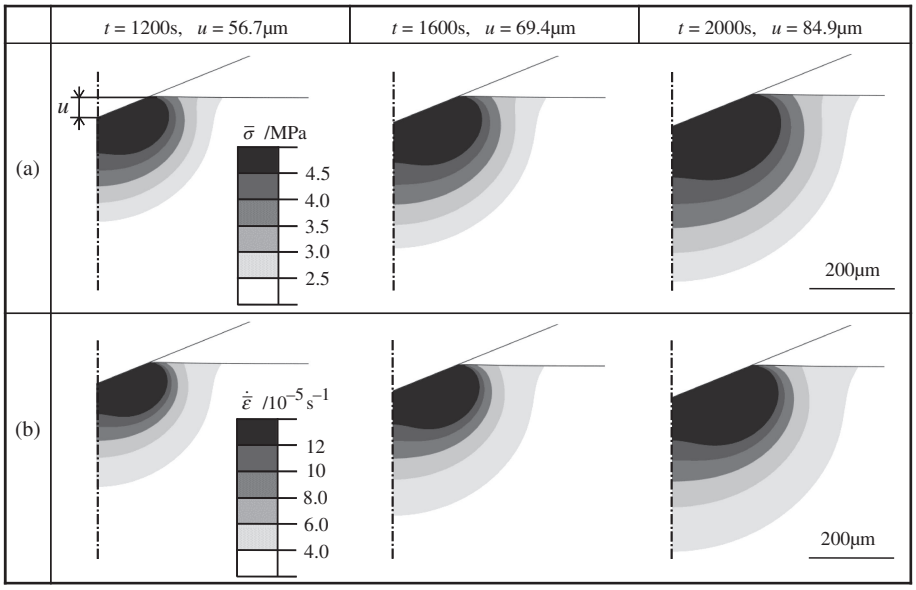

Fig. 4 Contours of (a) equivalent stress and (b) equivalent plastic strain rate. The contour lines expand toward the undeformed region while maintaining the geometrical self-similarity.

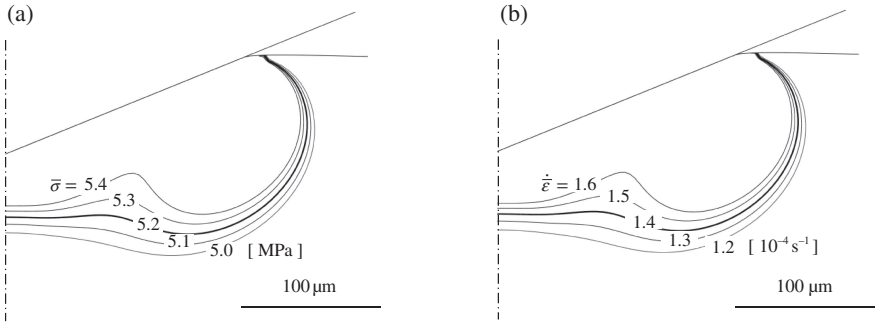

Fig. 5 Contours of (a) equivalent stress and (b) equivalent plastic strain rate. The thick curve shows the location of the representative points for the CV. These points are found on the curved surface having a shallow-bowl-like shape in three-dimensional space.

To evaluate the size of the CV, FE simulations were performed under the following deformation conditions:

$$\left.\begin{aligned} \bar{\sigma} > \left(\frac{\eta\dot{\bar{\varepsilon}}_r}{A}\right)^{1/3.0} \quad &\text{at} \quad \dot{\bar{\varepsilon}} = A\bar{\sigma}^{3.0}, \\ \bar{\sigma} \le \left(\frac{\eta\dot{\bar{\varepsilon}}_r}{A}\right)^{1/3.0} \quad &\text{at} \quad \dot{\bar{\varepsilon}} = 0. \end{aligned}\right\} \tag{16}$$

In the above equation, creep occurs in the whole region beneath the indenter at $\eta = 0$, and at $\eta = 1$, creep occurs only inside the CV representative surface. The results of FE simulation show that on the indentation creep curve of Fig. 1 ($\eta = 0$), $u = 85\,\mu$m at 2000 s, but when $\eta = 1$, $u = 68\,\mu$m is obtained at 2000 s. Therefore, the relative error r of the indenter displacement u when $\eta = 1$ is $r = 20\%$. Furthermore, in the pseudo-steady deformation state ($t \ge 1000$ s), r has the same value regardless of loading time. Here, for convenience, the size of the CV is estimated using $\eta = 0.02$, resulting in a relative error of 2% —that is, 1/10 the r value at $\eta = 1$. Thus, the CV is expressed as:

$$\dot{\bar{\varepsilon}} \ge \alpha/180. \tag{17}$$

The above equation indicates that CV decreases as the indentation creep rate ($\dot{\varepsilon}_{\mathrm{in(s)}} \cong \alpha$) increases. Furthermore, since the slope of $\dot{\bar{\varepsilon}}$ becomes steeper as the stress exponent increases, CV gets smaller.

4.5 Average strain within the control volume

Figure 6 shows the contour line pattern of the equivalent plastic strain rate $\dot{\bar{\varepsilon}}$ at $\alpha = 5.0 \times 10^{-4}\,\mathrm{s}^{-1}$, $t = 1600$ s. In the figure, the 3 contour lines of $\dot{\bar{\varepsilon}} = \dot{\bar{\varepsilon}}_r\eta$ (where $\dot{\bar{\varepsilon}}_r = 1.4 \times 10^{-4}\,\mathrm{s}^{-1}$, $\eta = 0.02$, 0.1 and 1) are drawn as solid lines. The contour line at $\eta = 1$ corresponds to the location of the CV representative points. Furthermore, the contour line at $\eta = 0.02$ represents the outside edge of the CV, and the interior of the CV is the area shown in gray. The diameter of the projected contact area of the indenter at this time is $d_0 = 344\,\mu$m, and the diameter of the CV on the sample surface is $d = 1389\,\mu$m. In the pseudo-steady deformation state ($t \ge 1000$ s), $d \cong 4d_0$ always holds true.

Next, we will look at the representative value of strain introduced by pressing the indenter (representative strain). If we determine the average by taking the sum of the products of the length of each element on the contour line at $\eta = 1$ and $\bar{\varepsilon}$ of that portion and dividing by the total length of the contour line, the result is $\langle\bar{\varepsilon}\rangle_{\eta=1} = 0.14$. At $\eta = 0.1$, it is $\langle\bar{\varepsilon}\rangle_{\eta=0.1} = 0.07$. Furthermore, if we determine the average by

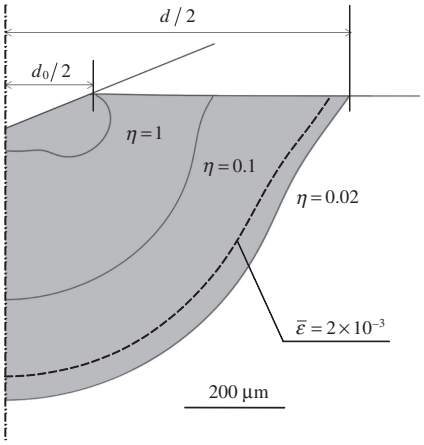

Fig. 6 Contours of equivalent plastic strain rate $\dot{\bar{\varepsilon}}$ at 1600 s. The CV is indicated by the area in gray. The dashed line shows the contour line for equivalent plastic strain $\bar{\varepsilon} = 2 \times 10^{-3}$.

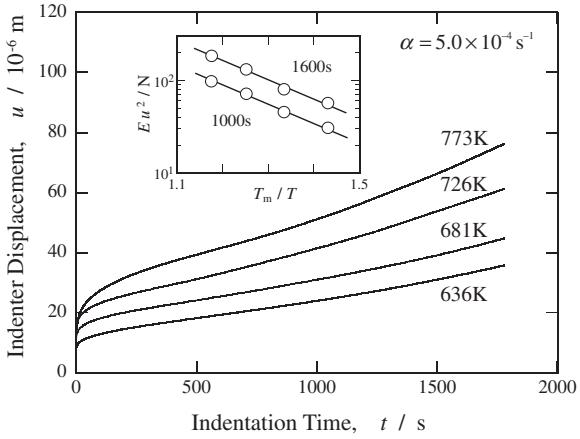

Fig. 7 Indentation creep curve for Al–5.3 mol% Mg solid-solution alloy. As shown in the inset, the semilogarithmic plots of Eu^2 versus T_m/T at the fixed loading time fall on a straight line.

taking the sum of the products of the area of each element within the CV and $\bar{\varepsilon}$ of that portion and dividing by the total area of the CV, the result is $\langle\bar{\varepsilon}\rangle_{CV} = 0.04$. These respective averages do not change as loading time elapses during the pseudo-steady deformation state. Branch *et al.*[26] performed FE simulation of hardness test of linear hardening materials and demonstrated that the average equivalent plastic strain (representative strain) in the deformation region of $\bar{\varepsilon} \geq 2.0 \times 10^{-3}$ underneath the Vickers indenter was $\bar{\varepsilon}_r \cong 0.035$. Since the positions of the contour line of $\bar{\varepsilon} = 2.0 \times 10^{-3}$ (dashed line) and the contour line of $\dot{\bar{\varepsilon}}$ at $\eta = 0.02$ in Fig. 6 are essentially the same, the value they obtained for $\bar{\varepsilon}_r$ agrees well with $\langle\bar{\varepsilon}\rangle_{CV} = 0.04$. However, Tabor[2] used $\varepsilon_r = 0.08$ as the representative strain introduced by the Vickers indenter, and Chaudhri[27] used $\varepsilon_r = 0.25$ to 0.36. Furthermore, Dao *et al.*[28] estimated the representative strain introduced by NanoIn testing at $\varepsilon_r = 0.033$. One reason that the representative strain values differ depending on the researcher in this manner is the individual differences in how they define it. In the present paper, we define the representative strain $\langle\bar{\varepsilon}\rangle_{CV}$ as the average value of equivalent plastic strain within the CV. Representative strain $\langle\bar{\varepsilon}\rangle_{CV} = 0.04$ is close to the values reported by Branch *et al.* and Dao *et al.*

4.6 Indentation creep test

Constant-pressure indentation creep tests were performed on an Al–5.3 mol% Mg solid-solution alloy using a micro-indenter. The indentation load was given by $F = F_0 \exp(2\alpha t)$, where $F_0 = 0.29$ N and $\alpha = 2.5 \times 10^{-4}$ to $4.0 \times 10^{-3}\,s^{-1}$. Figure 7 shows the indentation creep curves at each temperature at $\alpha = 5.0 \times 10^{-4}\,s^{-1}$. These curves have the same form as the results of the FE simulation in Fig. 1. When Eu^2 versus T_m/T at a certain loading time is plotted semilogarithmically as shown in the inset figure, the experimental data (open circles) fall on a straight line. This relationship always holds true in the pseudo-steady deformation state ($t \geq 1000$ s). From eq. (8), the slope of this straight line equals $-Q/2.3nRT_m$, and it depends on the ratio of activation energy Q and stress exponent n for creep. The fact that all experimental data fall on parallel lines suggests that indentation creep is governed by the same deformation-rate-controlling mechanism.

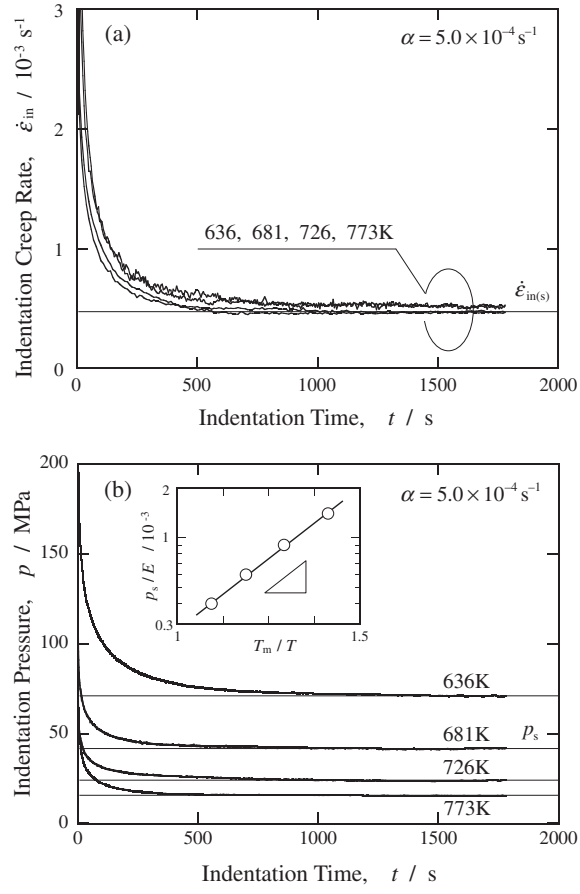

Fig. 8 (a) Time dependence of indentation creep rate. These results agree with the FE simulation results in Fig. 2. (b) The indentation pressure asymptotically approaches a constant value p_s after a certain loading duration. As shown in the inset, the semilogarithmic plots of p_s/E versus T_m/T fall on a straight line.

Figure 8(a) shows the change in indentation creep rate over time at each temperature. The indentation creep rate rapidly decreases immediately after loading, and when time reaches $t \geq 1000$ s, it approaches a constant value $\dot{\varepsilon}_{in(s)} \cong \alpha$. This experimental fact is consistent with eq. (11). These curves become one with no apparent dependence on

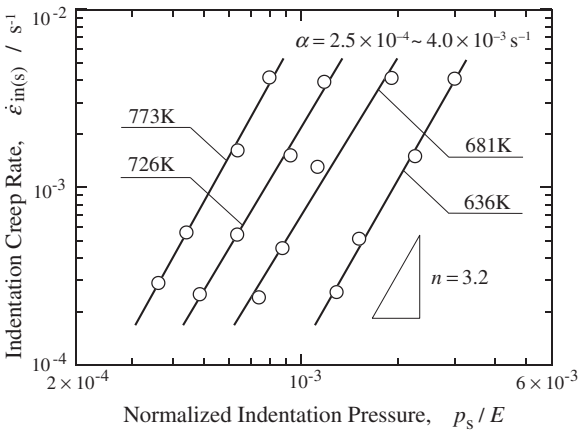

Fig. 9 Relationship of indentation creep rate $\dot{\varepsilon}_{in(s)}$ versus normalized indentation pressure p_s/E, both on logarithmic scales. All data fall on a group of parallel straight lines at each test temperature, and the slope of these lines corresponds to the stress exponent for creep n.

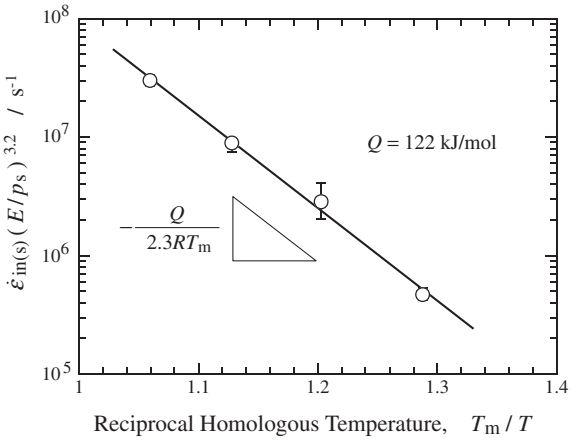

Fig. 10 Arrhenius plots of $\dot{\varepsilon}_{in(s)}(E/p_s)^n$, where $n = 3.2$. The activation energy for creep can be determined from the slope of this straight line.

temperature. This parallels the fact that eq. (9) does not include a temperature term. Figure 8(b) shows the change in indentation pressure over time. As is assumed from eq. (12), indentation pressure asymptotically approaches a constant value p_s fixed at each temperature. When these values are arranged as shown in the inset figure, the experimental data points (open circles) fall on one line. If the slope Δ of the straight line is equivalent to $Q/2.3nRT_m$ and the values of Δ and n are known, then Q can be estimated. In this case, $\Delta = 2.14$, and if $n = 3$, it is estimated that $Q = 112$ kJ/mol. We performed indentation creep tests in the range of $\alpha = 2.5 \times 10^{-4}$ to 4.0×10^{-3} s^{-1}, and those results showed that $\dot{\varepsilon}_{in(s)} \cong \alpha$ always holds true. It was also confirmed that p_s increases as the value of α increases, and decreases as temperature increases. These facts suggest that the pseudo-steady deformation state under the indenter is realized when $\dot{\varepsilon}_{in(s)}$ and p_s are constant.

4.7 Creep characteristic values

Figure 9 is a double-logarithmic plot of $\dot{\varepsilon}_{in(s)}$ and p_s/E obtained from constant-pressure indentation creep tests at $p_s = 13.9$ to 159 MPa. The open circles in the figure each represent the average of 3 experimental data points. These open circles fall on a different single straight line for each temperature. From eq. (13), the slope of this straight line is equivalent to the stress exponent for creep n. In this experiment, when $\bar{\sigma}_r = 4.6$ to 53 MPa, $n = 3.2 \pm 0.1$. This result agrees closely with the results of tensile creep tests by other researchers (Al–5.1 mol% Mg solid-solution alloy: $n = 2.8$ to 3.0 at $T = 601$ to 734 K, $\sigma = 4.9$ to 24.6 MPa,[29] Al–5.5 mol% Mg solid-solution alloy: $n = 3.1$ at $T = 673$ K, $\sigma = 9.8$ to 49.0 MPa[30]).

Figure 10 is an Arrhenius plot of the data (open circles) of Fig. 9. From eq. (14), the slope of this straight line is equivalent to $-Q/2.3RT_m$. The activation energy for creep determined from this slope is $Q = 122$ kJ/mol, which is close to the tensile creep test results of other researchers ($Q =$ 135 to 144 kJ/mol,[29] and $Q = 140$ kJ/mol[30]). This also agrees closely with the activation energy ($Q_d = 130$ kJ/mol) for diffusion of magnesium atoms in the aluminum matrix.[31] Judging from the creep characteristic values obtained in this study ($n = 3.2 \pm 0.1$, $Q = 122$ kJ/mol),[32,33] the creep rate of an Al–5.3 mol% Mg solid-solution alloy under these experimental conditions ($T = 636$ to 773 K, $\bar{\sigma}_r = 4.6$ to 53 MPa, and $\dot{\bar{\varepsilon}}_r = 6.9 \times 10^{-5}$ to 1.1×10^{-3} s^{-1}) is governed by the viscous glide of dislocations that drag the solute atmosphere.

4.8 Prediction of the constitutive equation for uniaxial creep

Figure 11 is a flow chart that explains the procedure for deriving the constitutive equation for conventional tensile creep or uniaxial creep from the results of an indentation creep test. (a) Perform a constant-pressure indentation creep test, and obtain the indentation creep curve $u = f(t)$. From this curve, determine the stress exponent n and activation energy Q for creep, and obtain the constitutive equation for indentation creep $\dot{\varepsilon}_{in(s)} = A(p_s/E)^n \exp(-Q/RT)$. (b) Perform FE simulation, and obtain the indentation creep curve $u = g(t)$. In the FE model, assume that power-law creep ($\dot{\bar{\varepsilon}} = B\bar{\sigma}^n$) occurs. Set the value of n in this model to the experimental result of step (a). Select an appropriate value of B such that $g(t) \cong f(t)$. (c) From the contour line pattern of equivalent stress, find the point where the representative stress of the CV is $\bar{\sigma}_r = C_1 p_s$ ($C_1 = 1/3$) (representative points), and examine the equivalent plastic strain rate thereof—that is, the representative strain rate $\dot{\bar{\varepsilon}}_r$. Determine the value of $C_2 = \dot{\bar{\varepsilon}}_r/\dot{\varepsilon}_{in(s)}$. However, the value of C_2 depends on the stress exponent n such that when $n = 3$, $C_2 = 0.28$, and when $n = 5$, $C_2 = 0.67$. This is done because if a correspondence table for n versus C_2 can be obtained beforehand, the FE simulation in step (b) can be omitted. (d) Using C_1 and C_2, calculate $\bar{\sigma}_r$ from p_s and $\dot{\bar{\varepsilon}}_r$ from $\dot{\varepsilon}_{in(s)}$. From these values of $\bar{\sigma}_r$ and $\dot{\bar{\varepsilon}}_r$, one can obtain the constitutive equation for conventional tensile creep or uniaxial creep $\dot{\bar{\varepsilon}}_r = A_0(\bar{\sigma}_r/E)^n \exp(-Q/RT)$.

In Fig. 12, the vertical axis is the Zener–Hollomon parameter ($Z_{in(s)} = \dot{\varepsilon}_{in(s)} \exp(122\,[\text{kJ/mol}]/RT)$ or $Z_r = \dot{\bar{\varepsilon}}_r \exp(122[\text{kJ/mol}]/RT)$), and the horizontal axis is p_s or $\bar{\sigma}_r$ normalized by the Young's modulus E at each temperature. The open circles are the data from Fig. 9 represented by line A. When p_s/E on this line is multiplied by $C_1 = 1/3$,

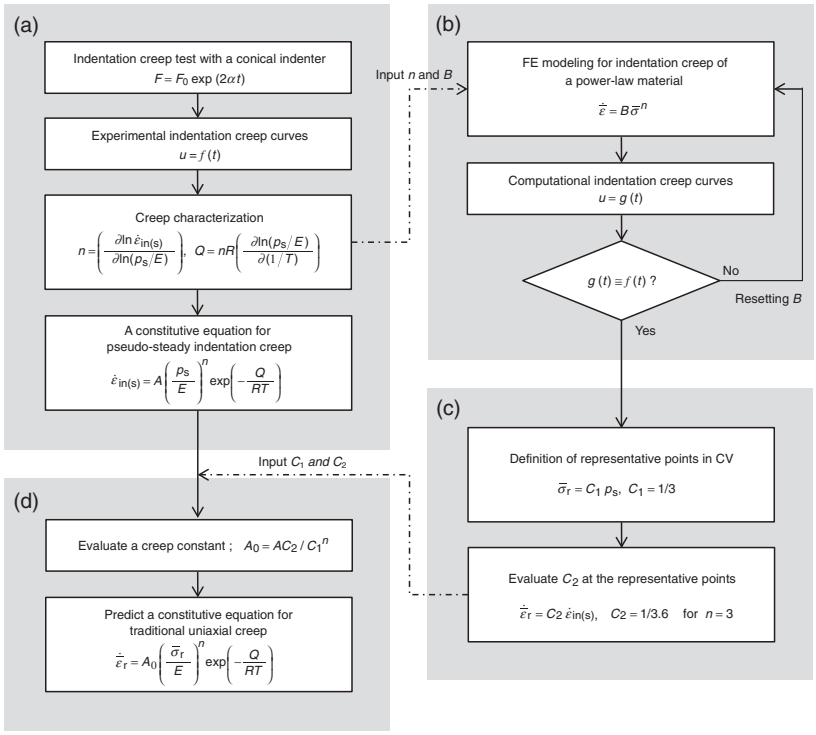

Fig. 11 Flow chart for predicting the constitutive equation for conventional uniaxial creep from the results of carefully designed indentation creep tests.

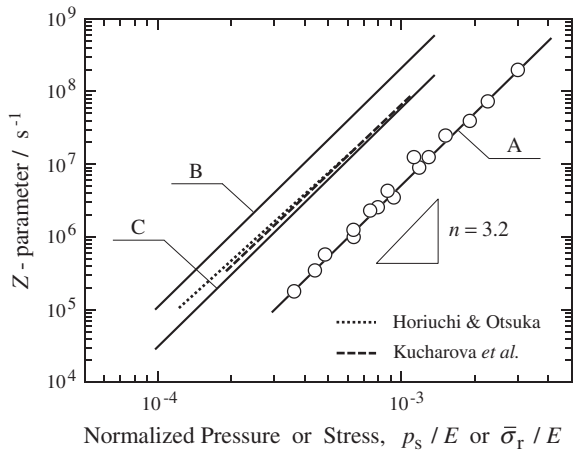

Fig. 12 Logarithmic plots of the Zener–Hollomon parameter versus p_s/E or $\bar{\sigma}_r/E$. All data (open circles) on line A are a redrawing of the results in Fig. 9. Line C, which is obtained from line A through line B, is in close agreement with the tensile creep results (shown by dotted and dashed lines) reported by other researchers.

the result is line B, which represents $Z_{in(s)}$ versus $\bar{\sigma}_r/E$. When $Z_{in(s)}$ on this line is multiplied by $C_2 = 1/3.6$, the result is line C, which represents Z_r versus $\bar{\sigma}_r/E$. Through this process, the constituent equation for conventional tensile creep or uniaxial creep is obtained:

$$\dot{\bar{\varepsilon}}_r = 1.12 \times 10^{16}\left(\frac{\bar{\sigma}_r}{E}\right)^{3.2} \exp\left(-\frac{122\,[\mathrm{kJ/mol}]}{RT}\right) \quad [\mathrm{s}^{-1}]. \tag{18}$$

The two lines represented by the dotted line and dashed line in the figure are the results of tensile creep test reported by other researchers.[29,30] It is clear from the figure, line C agrees well with the results of tensile creep test. This experimental fact shows that the constitutive equation for conventional tensile creep or uniaxial creep can be predicted with sufficient accuracy from the results of constant-pressure indentation creep test.

In this paper, we defined the CV representative points when the pseudo-steady deformation state occurs during indentation creep. It was demonstrated that by appropriately processing the experimental results, the results of an indentation creep test agree well with tensile creep test results. In practice, it is very important that the constitutive equation for uniaxial creep can be predicted through this method of testing and analysis. This method will play a key role in research and development of advanced light-weight heat-resistant structural materials that can only be obtained in small quantities.

5. Conclusion

Indentation creep experiments and FE simulations using an Al–Mg solid-solution alloy as a model material were performed in order to demonstrate that the constitutive equation for uniaxial creep (including all the creep parameter) can be predicted through the instrumented indentation testing technique. The main results are summarized as follows.

(1) When indentation pressure p and indentation creep rate $\dot{\varepsilon}_{in}$ are constant ($p \to p_s, \dot{\varepsilon}_{in} \to \dot{\varepsilon}_{in(s)}, \alpha$), the contour line patterns of equivalent stress $\bar{\sigma}$ and equivalent plastic strain rate $\dot{\bar{\varepsilon}}$ expand while maintaining geometrical self-similarity. The pseudo-steady deformation state is realized at this time.

(2) The deformation region just below the indenter in which the indenter velocity has been substantially

determined is called the control volume (CV). When the stress exponent for creep n is 3.0, $\dot{\bar{\varepsilon}} \geq \alpha/180$ is estimated for that region. The size of the CV decreases as the value of α increases.

(3) The location that represents creep behavior beneath the indenter is taken as the CV representative points. The representative stress at these points is $\bar{\sigma}_r = p_s/3$, and the representative strain rate is given by $\dot{\bar{\varepsilon}}_r = \alpha/3.6$ when $n = 3.0$. The average value of equivalent plastic strain within the CV is $\langle\bar{\varepsilon}\rangle_{CV} = 0.04$.

(4) When the pseudo-steady deformation state is realized in a constant-pressure indentation creep test, the values of the stress exponent and activation energy for creep extracted from this method are in good agreement with the results of conventional tensile creep tests.

(5) By appropriately processing the results of constant-pressure indentation creep tests, the constitutive equation (including all the creep parameter) for conventional tensile creep or uniaxial creep can be predicted with sufficient accuracy.

Acknowledgements

The indentation creep tests and FE simulations in this study were performed in collaboration with Y. Satoh and K. Ikemura, graduate students of Graduate School of Engineering at Nihon University. This work was partially supported by a Grant-in-Aid for Scientific Research (No. 22560660) from the Japan Society for the Promotion of Science (JSPS). M. Dao also acknowledges partial support from Singapore MIT Alliance (SMA).

REFERENCES

1) H. O'Neill: *The Hardness of Metals and Its Measurements*, (Chapman and Hall, London, 1934).
2) D. Tabor: *The Hardness of Metals*, (Oxford University Press, Oxford, 1951).
3) A. Gouldstone, N. Chollacoop, M. Dao, J. Li, A. M. Minor and Y.-L. Shen: Acta Mater. **55** (2007) 4015–4039.
4) A. C. Fischer-Cripps: *Nanoindentation*, (Springer-Verlag, New York, 2004).
5) P. J. Blau and B. R. Lawn: *Microindentation Techniques in Materials Science and Engineering*, (ASTM, Philadelphia, 1986).
6) T. O. Mulhearn and D. Tabor: J. Inst. Metal. **89** (1960) 7–12.
7) S. N. G. Chu and J. C. M. Li: Mater. Sci. Eng. **39** (1979) 1–10.
8) P. M. Sargent and M. F. Ashby: Mater. Sci. Technol. **8** (1992) 594–601.
9) M. Fujiwara: Japanese patent, No. 4096034.
10) M. Fujiwara: J. Japan Inst. Light Metals **52** (2002) 282–290.
11) M. Fujiwara and M. Otsuka: Mater. Sci. Eng. A **319–321** (2001) 929–933.
12) H. Takagi, M. Dao, M. Fujiwara and M. Otsuka: Philos. Mag. **83** (2003) 3959–3976.
13) H. Takagi, M. Dao, M. Fujiwara and M. Otsuka: Mater. Trans. **47** (2006) 2006–2014.
14) H. Takagi, M. Dao and M. Fujiwara: Acta Mech. Solida Sinica **21** (2008) 283–288.
15) B. N. Lucas and W. C. Oliver: Metall. Mater. Trans. A **30** (1999) 601–610.
16) Y. T. Cheng and C. M. Cheng: Philos. Mag. Lett. **81** (2001) 9–16.
17) T. H. Hyde, K. A. Yehia and A. A. Becker: Int. J. Mech. Sci. **35** (1993) 451–462.
18) A. F. Bower, N. A. Fleck, A. Needlman and N. Ogbonna: Proc. R. Soc. Lond. A **441** (1993) 97–124.
19) K. Abe, Y. Tanji, H. Yoshinaga and S. Morizumi: J. Japan Inst. Light Metals **27** (1977) 279–281.
20) E. A. Brandes and G. B. Brook: *Smithells Metals Reference Book*, (Oxford, Butterworth-Heinemann, 1992) Chap. 15, p. 2.
21) R. Hill: *Mathematical Theory of Plasticity*, (Oxford University Press, Oxford, 1950).
22) Y. T. Cheng and C. M. Cheng: Int. J. Solids Struct. **36** (1999) 1231–1243.
23) H. Kudo: *Soseigaku*, (Morikitashuppan, Tokyo, 1968).
24) M. Nakamura: *Katasasiken no Riron to Sonoriyouhou*, (Kougyo-chosakai, Tokyo, 2007).
25) H. M. Pollock, D. Maugis and M. Barquins: *Microindentation Techniques in Materials Science and Engineering*, eds. P. J. Blau and B. R. Lawn, (ASTM, Philadelphia, 1986) pp. 47–71.
26) N. A. Branch, G. Subhash, N. K. Arakere and M. A. Klecka: Acta Mater. **58** (2010) 6487–6494.
27) M. M. Chaudhri: Acta Mater. **46** (1998) 3047–3056.
28) M. Dao, N. Chollacoop, K. J. Van Vliet, T. A. Venkatesh and S. Suresh: Acta Mater. **49** (2001) 3899–3918.
29) R. Horiuchi and M. Otsuka: Mater. Trans. JIM **13** (1972) 284–293.
30) K. Kuchařová, I. Saxl and J. Čadek: Acta Metall. **22** (1974) 465–472.
31) E. A. Brandes and G. B. Brook: *Smithells Metals Reference Book*, (Oxford, Butterworth-Heinemann, 1992) Chap. 13, p. 16.
32) J. Cadek: *Creep in Metallic Materials*, (Elsevier, Amsterdam, 1988).
33) M. E. Kassner: *Fundamentals of Creep in Metals and Alloys*, (Elsevier, Amsterdam, 2009).